Ref. Ares(2025)1892070 - 10/03/2025

Deliverable D3.3

Atmospheric secondary aerosol formation from vehicle emissions in Europe and on a global scale

Pontus Roldin, Lund University

Matti Rissanen, Tampere University

PAREMPI
Particle emission prevention and impact: from real-world emissions of traffic to secondary PM of urban air

Funded by the European Union

PAREMPI Particle emission prevention and impact: from real-world emissions of traffic to secondary PM of urban air GRANT No: 101096133 (https://parempi.eu/)

PROJECT DURATION: 01/2023 – 12/2025

WP: WP3 Modelling of secondary aerosol formation and molecular level experiments

DELIVERABLE: D3.3 Atmospheric secondary aerosol formation from vehicle emissions in Europe and on a global scale

LEAD BENEFICIARY: Lund University

SUBMISSION DATE: 10-03-2025

DISSEMINATION LEVEL: Public

DUE DATE: M24, 31-12-2024

REVISION HISTORY:

DATE	VERSION	AUTHOR/CONTRIBUTOR	COMMENTS
15.02.2025	0.1	Pontus Roldin, Lund University Matti Rissanen, Tampere University	Initial draft
03.03.2025	0.2	Matti Rissanen, Tampere University	Review
06.03.2025	0.3	Päivi Aakko-Saksa, VTT	Final Quality Review
07.03.2025	1.0	Pontus Roldin, Lund University	Final version

CONSORTIUM:

ORGANISATION NAME	SHORT NAME	COUNTRY
VTT Technical Research Centre of Finland	VTT	Finland
Tampere University	TAU	Finland
Finnish Meteorological Institute	FMI	Finland
Automotive Research and Development Institute	BOSMAL	Poland
Lund University	ULUND	Sweden
Office national d'études et de recherches aérospatiales	ONERA	France
Institute of Experimental Medicine	IEM	Czechia
Magellan Circle	MAGELLAN CIRCLE	Portugal

Disclaimer

Funded by the European Union. Views and opinions expressed are however those of the author(s) only and do not necessarily reflect those of the European Union or CINEA. Neither the European Union nor the granting authority can be held responsible for them.

Table of Contents

1. Executive Summary 6
2. Introduction 7
3. Methods 7
   3.1 European scale model simulations 7
   3.2 Global scale model simulations 11
4. Results 11
   4.1 Particle number concentrations 12
   4.2 Road transport emissions impact on the nitrogen oxide and $PM_{2.5}$ levels in Europe 16
5. Outlook 19
6. References 20

List of abbreviations

ACDC	Atmospheric Cluster Dynamics Code
ACTRIS	The Aerosol, Clouds and Trace Gases Research Infrastructure
ADCHEM	Trajectory model for Aerosol Dynamics, gas and particle phase CHEMistry and radiative transfer
ASOA	Anthropogenic Secondary Organic Aerosol
BC	Black Carbon
BSOA	Biogenic Secondary Organic Aerosol
BTX	Benzene, Toluene and Xylene
CAMS	Copernicus Atmospheric Monitoring Service
CCN	Cloud Condensation Nuclei
CTM	Chemistry Transport Model
DMA	Dimethylamine
EMEP	European Monitoring and Evaluation Programme'
ePMI	equivalent total particles emissions index module
ESM	Earth System Model
GAINS	The Greenhouse gas - Air pollution Interactions and Synergies (GAINS) model
H_2SO_4	Sulfuric acid
HIA	Health Impact Assessment
HIO_2	Iodous acid
HIO_3	Iodic acid
HOM	Highly Oxygenated organic Molecules
HTAPv3	An emission inventory in support to Hemisperic Transport of Air Pollution version 3
HYSPLIT	The Hybrid Single-Particle Lagrangian Integrated Trajectory model
MCM	Master Chemical Mechanism
NEE	Non-Exhaust Emissions
NH_3	Ammonia
NO_x	Nitrogen oxides
NPF	New Particle Formation
OC	Organic Carbon
OH	Hydroxyl radicals
OP	Oxidative Potential
PAH	Polycyclic aromatic hydrocarbons
PNSD	Particle Number Size Distribution
PM_1	Particulate matter smaller or equal to 1 micron in diameter
$PM_{2.5}$	Particulate matter smaller or equal to 2.5 microns in diameter
PM_{10}	Particulate matter smaller or equal to 10 microns in diameter
PRAM	Peroxy Radical Autoxidation Mechanism
RI-URBANS	Research infrastructures services reinforcing air quality monitoring capacities in European urban and industrial areas
RO_2	Peroxy radicals

RO	Alkoxy radical
ROS	Reactive Oxygen Species
SMEAR	Station for Measuring Ecosystem-Atmosphere Relations
SIA	Secondary Inorganic Aerosol
SOA	Secondary Organic Aerosol
UFP	Ultrafine Particles
VBS	Volatility Basis Set
VOC	Volatile Organic Compounds

1. Executive Summary

This report describes the progress made on modelling vehicle emission impacts on the $PM_{2.5}$ and particle number concentrations in Europe and on a global scale during the first 24 months of the PAREMPI project. We have specifically focused on secondary organic and inorganic aerosol particle formation. The model results have been prepared to assess how vehicle emissions (road and ship traffic) impact the air quality, air pollution population exposure and population health (mortality and morbidity) in Europe.

2. Introduction

This public report describes the applied scientific methods and results from Task 3.4 - European and global scale estimates of the vehicle fleet contribution to organic and inorganic PM2.5 and nano-particle concentrations during all seasons in the PAREMPI project (Particle emission prevention and impact: from real-world emissions of traffic to secondary PM of urban air). We have performed extensive model simulations with the Lagrangian chemistry transport model ADCHEM using detailed gas-phase chemistry and secondary organic aerosol formation chemistry schemes developed in PAREMPI WP3. We have also implemented a novel new particle formation lookup table approach to represent new particle formation (NPF) involving sulfuric acid and ammonia in the global chemistry transport model TM5. The TM5 model was further used in the global Earth System Model EC-Earth v3 to assess the role of ammonia-sulfuric acid driven NPF.

3. Methods

3.1 European scale model simulations

In the PAREMPI project we have performed a comprehensive assessment of how road traffic and ship emissions influence the air pollution levels in Europe. The analysis was performed for the year 2018. This year was chosen because it is a reasonably recent year, before the less representative covid-19 pandemics year 2020, where we have access to the state-of-the-art anthropogenic emission inventories (CAMS, HTAPv3) and quality-controlled measurements from a large number of ACTRIS (Aerosol, Clouds and Trace Gases Research Infrastructure) stations and other measurement platforms (e.g. European Monitoring and Evaluation Programme': EMEP). These observations are used to evaluate the model results. To investigate the impact of road traffic and ship emissions on atmospheric chemistry and air pollution levels in Europe we basically performed three sets of chemistry transport model simulations:

1. Simulations that consider all state-of-the-art anthropogenic, biogenic and oceanic emissions of trace gases and aerosol particles (**Basecase**).
2. Simulations with the same model setup as in 1 but without road transport emissions (**WoRoad**).
3. Simulations with the same model setup as in 1 but without ship transport emissions (**WoShip**).

The modelled concentration differences between the **Basecase** simulations and the sensitivity simulations, **WoRoad** or **WoShip**, gives us information about how these anthropogenic emission sectors influence the air quality in different regions in Europe. The results from the model simulations presented in this report are further used in PAREMPI WP4 to assess how transport emissions influence the population health (mortality and morbidity) in Europe.

In PAREMPI the air pollution levels in Europe were simulated using the chemistry transport model (CTM) **ADCHEM**. ADCHEM is a type of Lagrangian chemistry transport model run along pre-calculated air mass trajectories (Roldin et al., 2011a-b; Roldin et al., 2019). In the model version used for the PAREMPI project the model represented the atmospheric boundary layer and lower free troposphere using 20 vertical layers, from the surface up to an altitude of 2.5 km (figure 1). ADCHEM simulates all aerosol dynamics processes (condensation, evaporation, coagulation, nucleation), wet and dry deposition and aerosol cloud droplet activation and processing. ADCHEM also has a near-explicit representation of how freshly emitted, externally mixed, soot agglomerates gradually collapse into compact, hygroscopic particles, i.e. Cloud Condensation Nuclei (CCN), when they are coated with secondary organic aerosol (SOA), secondary inorganic aerosol (SIA) material and water (Eriksson et al., 2017). ADCHEM explicitly simulates the temperature dependent multiphase chemistry and gas-molecular cluster-aerosol particle dynamics covering the complete size spectrum from vapor molecules and molecular clusters to larger aerosols and cloud droplets.

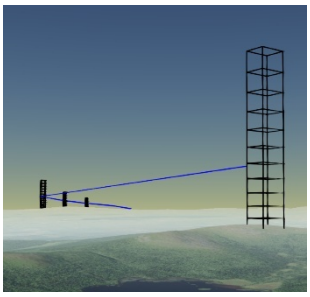

Figure 1. *Illustration of how the 1D-collumn model ADCHEM runs along an air mass trajectory.*

Secondary organic aerosol (SOA) formation*.* The gas-phase is fully coupled with the condensed-phase through the explicit representation of particle size dependent condensational growth and evaporation. The organic condensable vapours (in this case 1134 species, with a vapour pressure $<10^{-2}$ Pa at 298 K) are formed and degraded by near-explicit chemical reaction mechanisms based on the Master Chemical Mechanism (MCM) v3.3.1 (Jenkin et al., 1997; Jenkin et al., 2003; Saunder et al., 2003; Bloss et al., 2005; Jenkin et al., 2012; Jenkin et al., 2015) and the novel Peroxy Radical Autoxidation Mechanism (PRAM), further developed in PAREMPI (Roldin et al., 2019; Nie et al., 2023; Luo et al., 2024; Pichelstorfer et al., 2024). In total the implemented gas-phase chemistry mechanism considers 17,724 reactions and 6,308 species. All condensable organic vapours can partition reversibly between the gas-phase and condensed phase. In PAREMPI (Deliverable 3.2) we have further developed PRAM, which originally was developed to simulate the formation of Highly Oxygenated organic Molecules (HOM) and SOA during the ozonolysis and OH-oxidation of monoterpenes (Roldin et al., 2019; Nie et al., 2023; Luo et al., 2024). The new PRAM used for the ADCHEM simulations in PAREMPI also considers HOM formation from the major anthropogenic aromatic SOA precursors benzene (Pichelstorfer et al., 2024), toluene (Iyer et al., 2023) and unpublished mechanisms for *p*-,*o*- and *m*-xylene (BTX). The BTX PRAM development was performed utilizing our recently develop semi-automated peroxy radical autoxidation mechanism code (*i.e.*, automated alkoxy/peroxy radical autoxidation mechanism framework “autoAPRAM-fw” (Pichelstorfer et al., 2024).

The modelled SOA yields for BTX are within the relatively wide range of previously published SOA yields at low and high NO_x (Srivastava et al., 2022). However, more work is needed to evaluate the modelled SOA yields, volatility spectrum and chemical composition from BTX using novel observations from flow tubes and smog chamber experiments. For other important anthropogenic SOA precursors, including other single ring aromatic compounds (e.g. ethylbenzene, trimethylbenzenes), polycyclic aromatic hydrocarbons (PAH) (e.g. naphthalene and anthracene) and alkanes (e.g. dodecane), we did not implement detailed gas-phase oxidation and SOA formation mechanisms within this timeframe (see more details in the PAREMPI D3.2 report). Hence, most likely the ADCHEM model version used for this report underestimates the anthropogenic SOA mass formation.

Atmospheric New Particle Formation (NPF). ADCHEM is the first atmospheric chemistry transport model that represents the gas-molecular cluster aerosol dynamics that governs the atmospheric new particle formation explicitly. This is performed with the novel **ClusterIn** module (Olenius and Roldin, 2022), which serves as an extension of the aerosol dynamics models down to molecular cluster sizes, thus enabling the simulation of the time evolution of the complete molecular cluster and aerosol particle size range. The numerical solution of the cluster concentrations is conducted by the atmospheric cluster dynamics code **ACDC** (Olenius et al., 2013), embedded in the ClusterIn framework. ACDC solves the time evolution of a population of molecular clusters considering all possible collision and evaporation processes between the clusters and vapor molecules. The rate constants related to cluster growth and evaporation are calculated using quantum chemical data. In the model simulations performed for this report we considered ion-mediated NPF via clusters of NH_3-H_2SO_4, DMA-H_2SO_4 and HIO_2-HIO_3, in line with recent ADCHEM publications (Xavier et al., 2024; Wollesen de Jonge et al., 2024). The detailed gas-molecular cluster-aerosol dynamics make ADCHEM ideally suitable for studies of ultrafine particles (UFP), i.e. aerosol particles smaller than 100 nm in diameter.

ADCHEM pre-processing. ADCHEM was set up and run along air mass trajectories generated with the Hybrid Single-Particle Lagrangian Integrated Trajectory model **HYSPLIT** (Stein et al., 2015). HYSPLIT was applied to trace the transport patterns and aerosol emission source regions for 51 stations (receptor locations) in Europe (Table 1), using similar methods as in previous ADCHEM publications (Roldin et al., 2019; Wollesen de Jonge et al., 2024; Xavier et al., 2024). We have developed efficient ADCHEM pre-processing scripts that load meteorological variables and emissions among other parameters along the generated air mass trajectories. For this report we used global ocean and biogenic emission inventories with a resolution of 0.1° from the Copernicus Atmosphere Monitoring Service (CAMS) (Granier et al., 2019) and anthropogenic global emissions with a resolution 0.1° from HTAPv3 (Crippa et al., 2023). HTAPv3 was chosen primarily because this emission inventory, in contrast to CAMS, includes non-exhaust road transport emissions (NEE). However, in the PAREMPI project we have also run complementary model simulations using the CAMS anthropogenic emission inventory. The CAMS and HTAPv3 anthropogenic emissions differ significantly especially concerning the emissions of organic carbon (OC) and black carbon (BC) from residential combustion and international shipping, where HTAPv3 gives significantly higher BC emissions.

Primary particle number emission factors. The size resolved anthropogenic primary particle number emissions, in the diameter size range 3 nm to 10 µm, were estimated using the existing global continental anthropogenic PM_1 primary particle number emission inventory from Paasonen et al. (2016) and emission sector specific PM_1:$PM_{2.5}$ and $PM_{2.5}$:PM_{10} emission factors from the GAINS model (Amann et al., 2011). Recent ambient measurements in urban regions have also demonstrated that road traffic is a significant source of primary UFPs in the size range 1 nm to 10 nm in diameter (Lintusaari et al. 2023, Olin et al. 2023). Hence for the model simulations presented in this report we used the reported average road transport fleet emission factors of UFPs in the size range between 1 nm and 10 nm in diameter from Lintusaari et al. (2023), reported as particle number emission factors per kg of CO_2 emitted. The CO_2 emissions from the road traffic was taken from the global CAMS emission inventory v5.3.

***Remapping the concentrations on a fixed spatial domain*.** To be able to link the modelled air pollutant concentrations from ADCHEM to population exposure and health effects the modelled concentrations along the individual air mass trajectories need to be remapped and averaged on a fixed spatial grid. In the PAREMPI project the modelled concentrations along

all air mass trajectories were remapped onto a spatial grid domain of 0.25°x0.25° over Europe. 486 air mass trajectory simulations, evenly distributed over the year (one new trajectory every 18th hour), were performed for each station, starting 10 days upwind and continuing 1 day downwind the stations. In total this results in 24 786 individual ADCHEM simulations. Based on all trajectory simulations we calculated detailed 3D-concentration fields, comparable with a 3D-Eulerian model, but with much more detailed information about the chemistry and physical aerosol properties than a 3D-CTM can accomplish. The model results over the full European domain are presented as average seasonal or yearly concentration fields while for the targeted stations (Table 1) we can provide 18 h resolution time series over the full year of 2018 (see e.g. figure 2B).

Table 1. *List of targeted stations for the ADCHEM air mass trajectory simulations in PAREMPI. The majority of the stations are part of the ACTRIS and EMEP station networks, while others are SMEAR stations (https://www.atm.helsinki.fi/smear/) and/or RI-URBAN stations (https://riurbans.eu/). Four additional urban stations in Rome, Warsaw, Istanbul and Lund, which are not part of these international station networks were also included to provide better spatial coverage. Most of the stations are either regional background (RB) or urban background (UB) air quality stations. Only two stations Hornsgatan in Stockholm and Trollebergsvägen in Lund are located next to busy roads and are thus classified as Traffic (TR) sites.*

Station name	Coordinates	Country	EMEP-code	Description*
Pallas	67.9733 °N, 24.1161 °E	Finland	FI0096G	RB, ACTRIS
Värriö	67.7667 °N, 29.5833 °E	Finland	FI0023R	RB, ACTRIS
Bredkälen	63.8500 °N, 15.3333 °E	Sweden	SE0005R	RB, EMEP
Puijo	62.9108 °N, 27.6557 °E	Finland		RB, SMEAR
Kårvatn	62.7833 °N, 8.8833 °E	Sweden	NO0039R	RB, ACTRIS
Hyytiälä	61.8500 °N, 24.2833 °E	Finland	FI0050R	RB, ACTRIS, SMEAR
Helsinki	60.2029 °N, 24.9612 °E	Finland	FI0038U	UB, RI-URBANS, SMEAR
Norunda	60.0864 °N, 17.4794 °E	Sweden	SE0023R	RB, ACTRIS
Utö	59.7792 °N, 21.3772 °E	Finland	FI0009R	RB, marine
Stockholm, Hornsgatan	59.3171 °N, 18.0484 °E	Sweden	SE0024U	TR, RI-URBANS
Birkenes II	58.3885 °N, 8.2520 °E	Norway	NO0002R	RB, ACTRIS
Hyltemossa	56.0976 °N, 13.4190 °E	Sweden	SE0021R	RB, ACTRIS
Rucava	56.1619 °N, 21.1731 °E	Latvia	LV0010R	RB, EMEP
Auchencorth	55.7922 °N, -3.2429 °E	Scottland	GB0048R	RB, ACTRIS
Lund, Trollebergsvägen	55.7760 °N, 13.0480 °E	Sweden		TR
Diabla Gora	54.1500 °N, 22.0667 °E	Poland	PL0005R	RB, EMEP
Mace Head	53.3258 °N, -9.8994 °E	Ireland	IE0031R	RB, EMEP
Neuglobsow	53.1413 °N, 13.0317 °E	Germany	DE0007R	RB, ACTRIS
Waldhof	52.8022 °N, 10.7594 °E	Germany	DE0002R	RB, ACTRIS
Warsaw	52.2223 °N, 21.0083 °E	Poland		UB
Cabauw	51.9703 °N, 4.9264 °E	Netherlands	NL0644R	RB, ACTRIS
Melpitz	51.5255 °N, 12.9277 °E	Germany	DE0044R	RB, ACTRIS
Mülheim-Styrum	51.4535 °N, 6.8651 °E	Germany	DE0069B	UB
Leipzig	51.3525 °N, 12.4346 °E	Germany	DE0055B	UB, ACTRIS
Chilbolton	51.1496 °N, -1.4382 °E	England	GB1055R	RB, ACTRIS
Dresden-Winckelmannstrasse	51.0361 °N, 13.7306 °E	Germany	DE0064B	UB, RI-URBANS
Villeneuve d'Ascq	50.6110 °N, 3.1404 °E	France	FR0027U	UB, ACTRIS
Langen	50.0050 °N, 8.6514 °E	Germany	DE0065B	UB, RI-URBANS
Kosetice	49.5734 °N, 15.0803 °E	Czech Rep.	CZ0003R	RB, ACTRIS
Stará Lesná	49.1500 °N, 20.2833 °E	Slovakia	SK0004R	RB, EMEP
SIRTA (Paris)	48.7089 °N, 2.1487 °E	France	FR0020R	RB/UB, ACTRIS,
Observatoire Perenne de l'Environ.	48.5622 °N, 5.5056 °E	France	FR0022R	RB, ACTRIS
Hohenpeissenberg	47.8015 °N, 11.0096 °E	Germany	DE0043G	RB, ACTRIS
K-puszta	46.9653 °N, 19.5449 °E	Hungary	HU0002R	RB, ACTRIS
La Tardière	46.6500 °N, -0.7500 °E	France	FR0015R	RB, EMEP
Leova II	46.4884 °N, 28.2835 °E	Moldova	MD0013R	RB, EMEP
Ispra	45.8146 °N, 8.6357 °E	Italy	IT0004R	RB, ACTRIS
Puy De Dôme	45.7722 °N, 2.9649 °E	France	FR0030R	RB, ACTRIS
Kamenicki vis	43.4000 °N, 21.9500 °E	Serbia	RS0005R	RB, EMEP

Marseille	43.3053 °N, 5.3947 °E	France	FR0035U	UB, RI-URBANS
Noia	42.7210 °N, -8.9240 °E	Spain	ES0005R	RB, EMEP
Villa Ada (Rome)	41.9300 °N, 12.5100 °E	Italy		UB
Montseny	41.7667 °N, 2.3500 °E	France	ES1778R	RB, ACTRIS
Beşiktaş (Istanbul)	41.0440 °N, 29.0130 °E	Turkey		UB
Madrid	40.4564 °N, -3.7256 °E	Spain	ES0021U	UB, ACTRIS
Lecce	40.3358 °N, 18.1245 °E	Italy	IT0017U	UB, ACTRIS
DEM Athens	37.9950 °N, 23.8160 °E	Greece	GR0100B	RB/UB, ACTRIS
Granada	37.1640 °N, -3.6050 °E	Spain	ES0020U	UB, ACTRIS
El Arenosillo	37.1000 °N, -6.7333 °E	Spain	ES0100R	RB, ACTRIS
Finokalia	35.3378 °N, 25.6694 °E	Greece	GR0002R	RB, marine, ACTRIS
Agia Marina Xyliatou	35.0381 °N, 33.0578 °E	Cyprus	CY0002R	RB, marine, ACTRIS

3.2 Global scale model simulations

In PAREMPI WP3 we are developing a novel digital equivalent total particles emissions index module (ePMI) software which is intended to be implemented and used in global, and regionals scale Eulerian CTM and ESM models for improved representation of primary and secondary aerosol particle number and mass formation from anthropogenic sources, with focus on the transport sectors. The ePMI module includes simplified parameterizations of biogenic and anthropogenic SOA and UFP formation rates based on a limited number of input variables ([NO_x], [O_3], [OH], [H_2SO_4], VOC mixtures, [NH_3], temperature *etc*), which are standard variables provided by regional and global scale CTM. The ePMI module is based on the existing and widely used modal aerosol dynamics module (M7) (Vignati et al., 2004; van Noije et al., 2014), improved anthropogenic SOA volatility basis set (VBS) parameterizations developed in PAREMPI, and novel NH_3-H_2SO_4 NPF lookup tables based on **ACDC** (Olenius et al., 2013). We have implemented and tested the NPF lookup table together with M7 in ADCHEM and the global ESM/CTM EC-Earth/TM5 (Svenhag et al., 2024a; Svenhag et al., 2024b), and we are currently working on the evaluation and implementation of simplified representations of anthropogenic SOA VBS schemes, analogous to the existing biogenic SOA formation schemes used in EC-Earth/TM5 (Bergman et al., 2022, Svenhag et al., 2024a; Svenhag et al., 2024b). One major challenge that we face is how to reasonably accurately represent the anthropogenic NO_x emissions influence on the non-linear peroxy/alkoxy radical (RO_2/RO) oxidation chemistry that regulates the SOA volatility and yields (e.g. Ng et al., 2007; Nie et al., 2023). We currently explore the possibility to train a neural network (NN) to predict the difference in the volatility distribution (i.e. VBS) of VOC oxidation products from the detailed chemistry module developed and used in ADCHEM (PAREMPI deliverable 3.2) and the simplified schemes used e.g. in TM5, at variable atmospheric conditions (temperature, [NO_x], VOC mixtures, [OH], [O_3]) (Vartiainen et al., 2024). Finaly we will correct the biases caused by the simplified formulation and implement this revised parametrization into the ePMI module.

4. Results

In this report we present model results from ADCHEM simulations over Europe for year 2018 and provide examples of how the model results are being evaluated with existing observations from the targeted monitoring stations in Europe (Table 1). Further we give examples of how road transport emissions influenced the air quality in Europe in 2018. The results from these

model simulations will be part of several research article manuscripts and conference presentations.

4.1 Particle number concentrations

Figure 2 and 3 shows examples of the modelled (Basecase) and observed particle number size distributions (PNSD) and total concentrations of particles larger than 10 nm in diameter ($PN(D_p> 10nm)$) in 2018 at the regional background stations Hyltemossa in Southern Sweden and Ispra in Northern Italy. At Hyltemossa the measured and modelled yearly average $PN(D_p> 10nm)$ were 2028 cm^{-3} and 2017 cm^{-3}, respectively. The particle number concentrations increase significantly during the spring and summer months, likely because of photochemical induced NPF. During May-August the measured and modelled average $PN(D_p> 10nm)$ were 2728 cm^{-3} and 2947 cm^{-3} while during the winter months (Jan-Feb and Nov-Dec) the average measured and modelled $PN(D_p> 10nm)$ were 1267 cm^{-3} and 1052 cm^{-3}, respectively. At Ispra, in the polluted Po Valley, ~50 km Northwest from Milan, the yearly average measured and modelled $PN(D_p> 10nm)$ were 7174 cm^{-3} and 5791 cm^{-3}, respectively. In contrast to Southern Sweden, the observed particle number concentrations are significantly higher during the winter months compared with the summer months at Ispra. The measured and modelled average $PN(D_p> 10nm)$ during the winter months (Jan-Feb and Nov-Dec) were 8595 cm^{-3} and 6181 cm^{-3}, while during the summer months (May-Aug) the average measured and modelled $PN(D_p> 10nm)$ were 5872 cm^{-3} and 5425 cm^{-3}, respectively. The reason why the model underestimates the particle number concentrations during the winter months at Ispra can possibly be attributed to underestimated primary particle emissions, e.g. from residential heating and/or underestimated road traffic particle emission factors during the colder winter months. However, it can also be a result of stable atmospheric conditions (shallow inversion), which most likely is not fully captured by the model. The shape of the modelled median PNSD at these two stations are generally in reasonable agreement with the observations, with an Aitken mode peaking at between 60 and 90 nm in diameter. The exception is the winter months at Hyltemossa (figure 2D) when the observed PNSD is clearly bimodal, with a Hoppel minima (Hoppel et al., 1986), indicating significant influence from aerosol cloud droplet activation and particle growth. The Hoppel minima is not fully captured by the model.

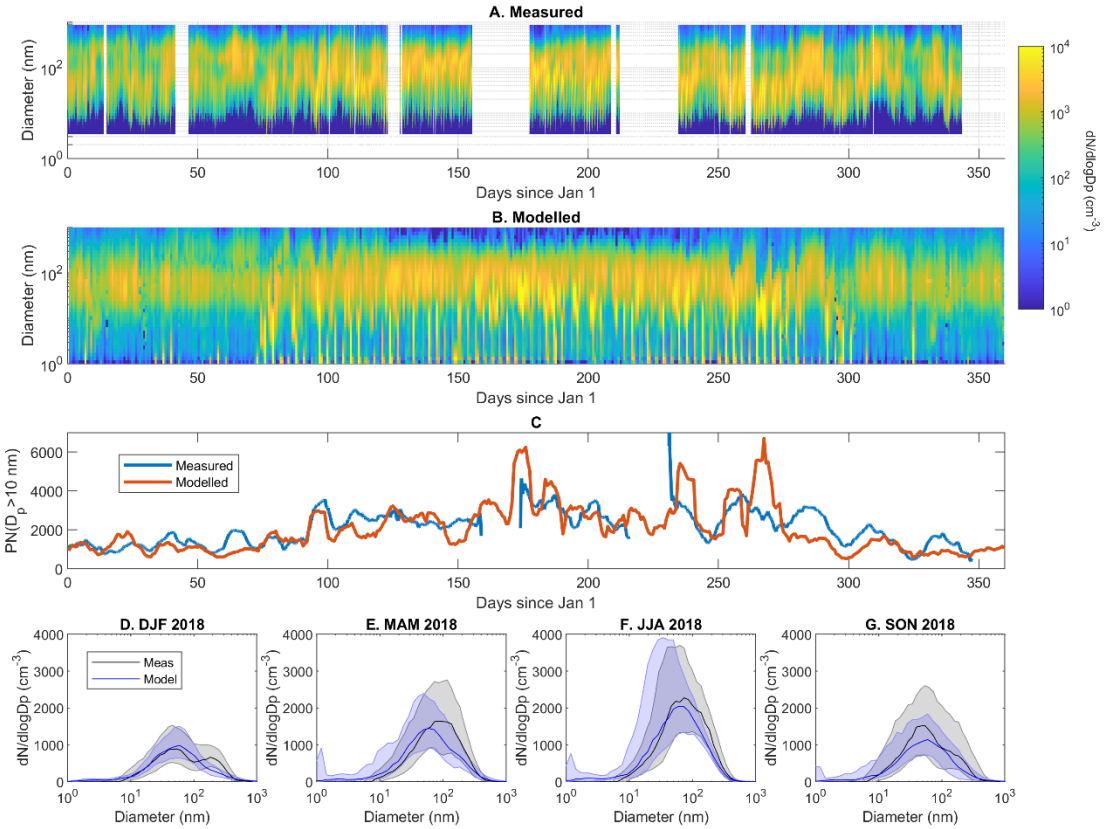

***Figure 2**. Measured and modelled submicron particle number size distributions at the regional background station Hyltemossa in Southern Sweden in 2018. Panels **A** and **B** show the measured and modelled particle number size distribution time series for the entire year. Panel **C** shows 7-days moving average total concentrations of particles larger than 10 nm in diameter. Panels **D**-**G** show the measured and modelled median and 25-75 percentile particle number size distributions for December-January-February (DJF), March-April-May (MAM), June-July-August (JJA) and September-October-November (SON).*

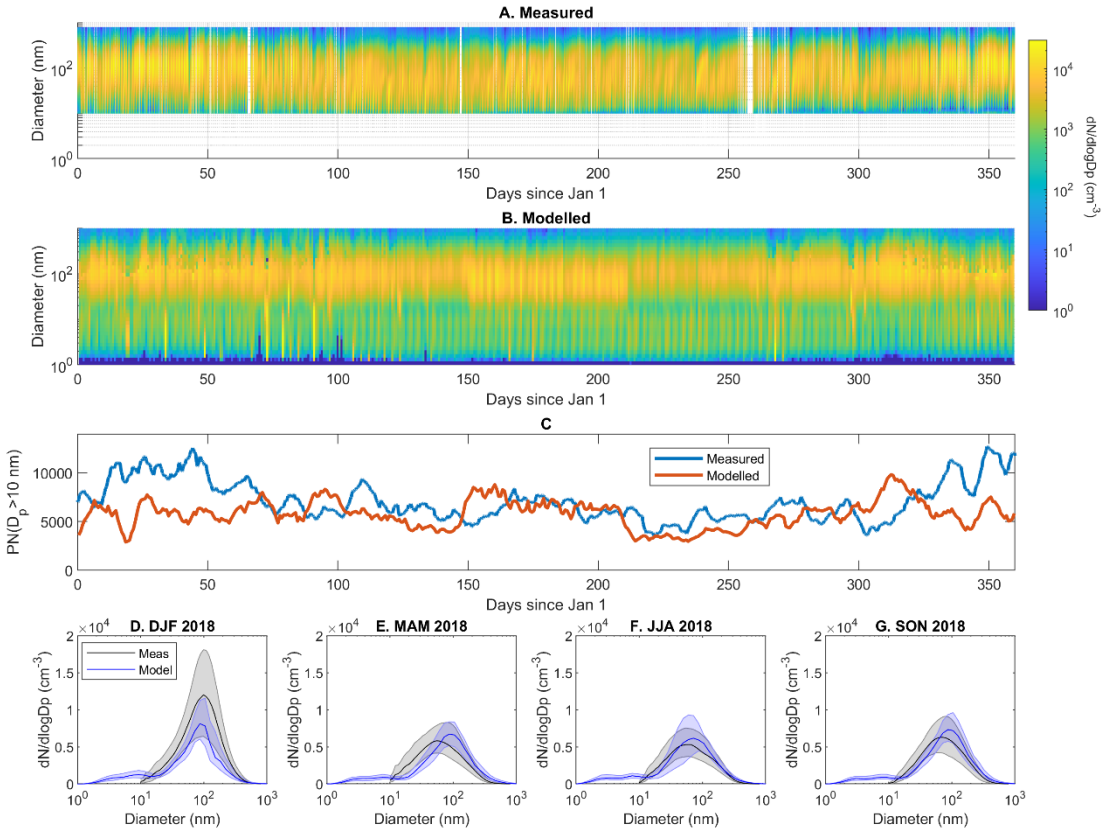

***Figure 3**. Measured and modelled submicron particle number size distributions at the regional background station Ispra in Northern Italy. Panels **A** and **B** show the measured and modelled particle number size distribution time series for the entire year. Panel **C** shows 7-days moving average total concentrations of particles larger than 10 nm in diameter. Panels **D**-**G** show the measured and modelled median and 25-75 percentile particle number size distributions for January-February (JF), March-April-May (MAM), June-July-August (JJA) and September (Sep). No PNSD observations are available from October, November and December 2018.*

As part of the ongoing work with the PAREMPI ePMI software (PAREMPI Deliverable 3.4) we have also evaluated how the global ESM EC-Earth can represent the seasonal and diurnal trends in the PNSD. The results from EC-Earth were benchmarked against model simulations with ADCHEM and observations from the ACTRIS stations Hyltemossa, Sweden and Hyytiälä, Finland (Svenhag et al., 2024b). Although ADCHEM does not always capture the dynamics of individual NPF event days, the seasonal trends in the observed PNSD and UFP at these regional background stations are well represented by the model (Svenhag et al., 2024b, Wollesen de Jonge et al., 2024, and figure 2). With EC-Earth we have shown that the novel NH_3-H_2SO_4 NPF lookup table approach increases the modelled total particle number concentrations and CCN concentrations significantly (Svenhag et al., 2024a; Svenhag et al., 2024b), but the model still underestimates the particle number concentrations and the particle growth into the Aitken/accumulatio mode size range between March to October (Svenhag et al., 2024b). This may partly be due to missing condensable organic vapours in the model. Presently EC-Earth does not account for anthropogenic SOA formation.

Figure 4 shows the compiled modelled yearly average UFP and PN(D_p>100 nm) concentrations in the atmospheric surface layer over Europe in 2018. The impact from ship emissions on the UFP concentrations along the major ship lanes are clearly apparent in the Adriatic Sea, Mediterranean Sea, the North Atlantic Ocean, English Channel, North Sea and the Baltic Sea (figure 4A), with major impact on the UFP levels over the ocean and coastal

regions in Europe. For particles larger than 100 nm in diameter the geographical concentration patterns look markedly different, with hotspot regions in the Po Valley in Northern Italy (see also figure 3) and East Europe, in particularly over the Balkan countries (figure 4B). Figures 4C-F show examples of modelled and measured yearly average median PNSD and corresponding 10-90 percentile PNSD for a few selected ACTRIS stations in Europe.

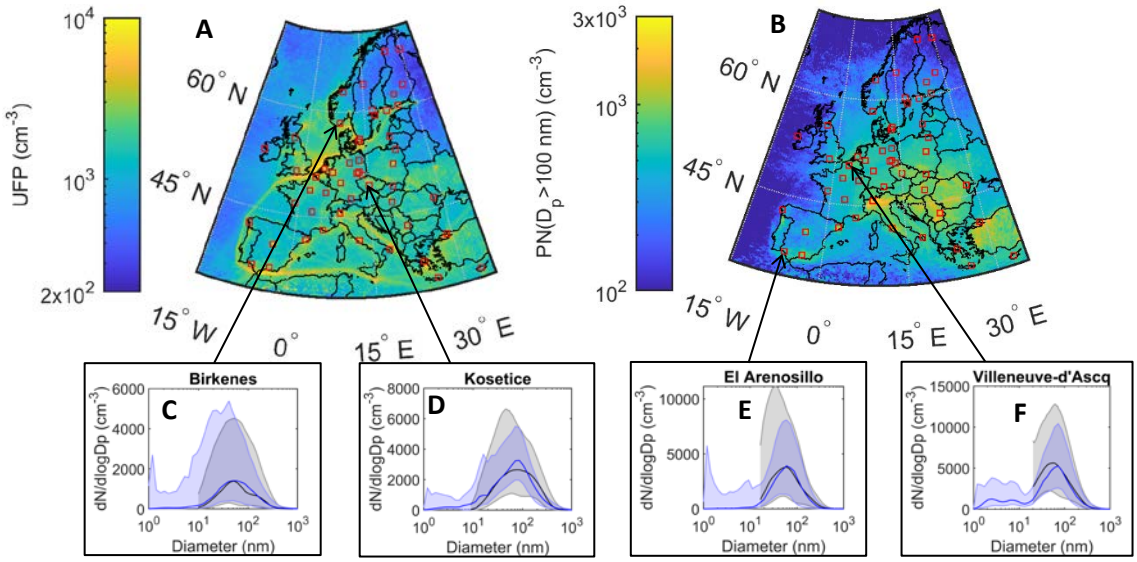

Figure 4. *Modelled (ADCHEM) average surface concentrations of UFP (panel **A**) and particles >100 nm in diameter (panel **B**) in Europe in year 2018. Panel **C**-**F** compares modelled (blue) and measured (black) PNSD at selected stations in Norway, Czech Republic, Spain and France (shaded covers the 10-90 percentile PNSD range). The red square symbols show the location of the 51 receptor locations (stations) that ADCHEM was run to (Table 1).*

To investigate how different emission sectors and processes (e.g. NPF) influence the particle concentrations in different regions in Europe we performed several ADCHEM sensitivity model runs. Considering the scope of the PAREMPI project, the most extensive sensitivity simulations, covering all regions over the European continent, were performed to assess how road and ship emissions influence the air quality. However, for selected regions (stations) we also investigated how other anthropogenic emission sectors (e.g. residential heating) impacts the concentrations. Figure 5 shows an example of the modelled PNSD from such model sensitivity simulations targeting an urban background station in Lecce, Southern Italy. Even when considering all known particle emission sources and processes, including novel road traffic UFP emission factors (Lintusaari et al. 2023), the model tends to underestimate the observed UFP concentrations below ~30 nm in diameter. A likely reason for this is the applied relatively coarse resolution anthropogenic emission inventory of 0.1°x0.1° that does not capture local urban hotspot particle emissions. Hence, for most urban stations the applied European scale ADCHEM model setup tends to underestimate the UFP concentrations, while the model generally captures the observed regional background UFP levels reasonably well (see e.g. figure 2, 3 and 4C-E). At the urban background station in Lecce (~15 km from the Adriatic Sea), ship traffic and residential heating have major impact on the modelled yearly median Aitken/accumulation mode particle number concentrations when using the HTAPv3 emission inventory, while road traffic mainly impacts the sub 10 nm particle number concentrations. On a yearly basis regional NPF events seem to have minor impact on the median particle number concentrations at this urban station according to the model.

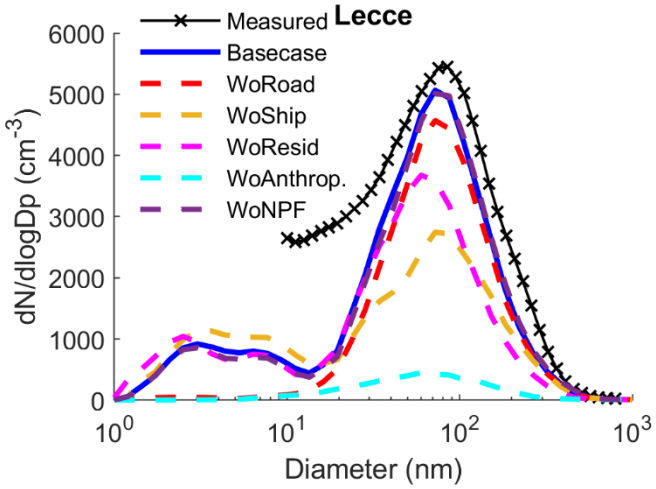

***Figure 5**. Example of modelled and measured yearly average PNSD at the urban background ACTRIS station in Lecce in Southern Italy in 2018. Apart from the results from the base case model simulations the figure shows the median PNSD from simulations without emissions from road traffic (WoRoad), ships (WoShip), residential heating (WoResid) and without any anthropogenic emissions (WoAnthrop). We also performed simulations without NPF (WoNPF).*

4.2 Road transport emissions impact on the nitrogen oxide and $PM_{2.5}$ levels in Europe

According to the ADCHEM model simulations the road traffic in Europe has major impact on the nitrogen oxides ($NO_x \equiv NO + NO_2$) levels and indirectly on the ozone and PM levels (nitrate aerosol mass) in central Europe and urban regions in general. Figure 6A shows the modelled yearly average NO_x levels and figure 6B the road traffic contribution to the NO_x levels according to our model simulations using the HTAPv3 emission inventory. Similar trends are also seen in the road traffic emissions contribution to the modelled $PM_{2.5}$ levels (figure 7).

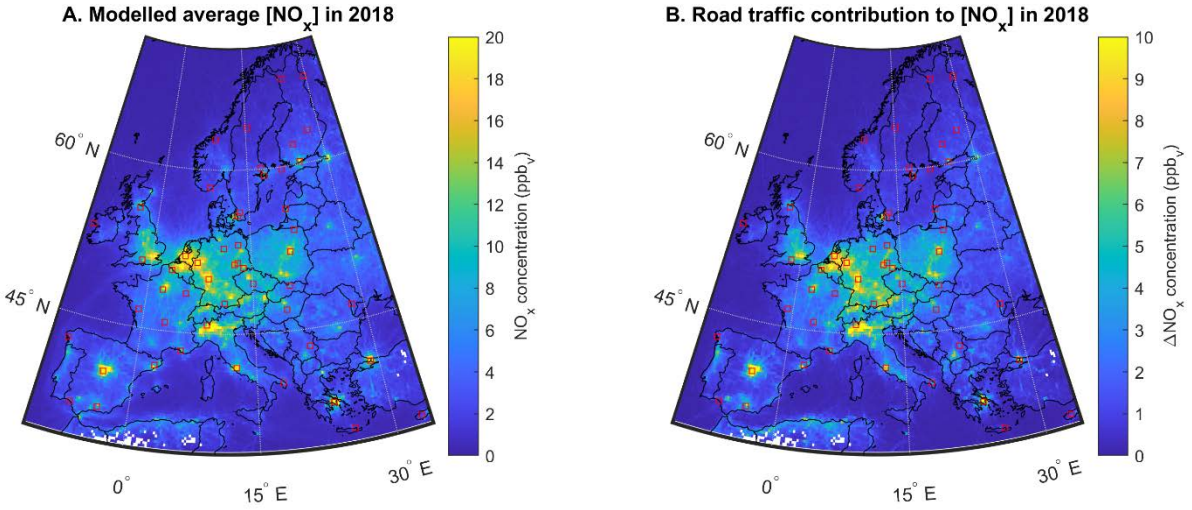

***Figure 6**. Modelled average NO_x concentrations over Europe in the year 2018. Panel **A** shows the absolute concentrations from the Basecase model simulations. Panels **B** show the concentration difference between the Basecase and the WoRoad simulations. The red square symbols show the location of the 51 receptor locations (stations) that ADCHEM was run to (Table 1). Note that the colorbar scales are different in panel A and B.*

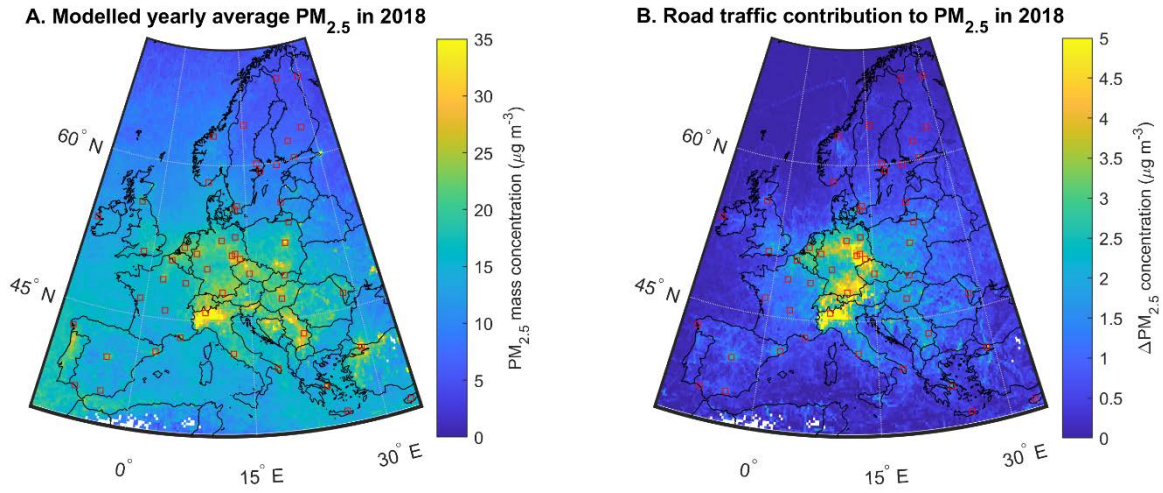

***Figure 7**. Modelled average $PM_{2.5}$ levels over Europe in the year 2018. Panel **A** shows the absolute concentrations from the Basecase model simulations. Panels **B** show the concentration difference between the Basecase and the WoRoad simulations.*

Most of the $PM_{2.5}$ mass from road traffic is nitrate PM (figure 8) formed as SIA from the road traffic NO_x emissions. A smaller share of the road traffic emissions contribution to the $PM_{2.5}$ levels in Europe are BC, primary organic aerosol (POA) and NEE (figure 9). According to our model simulations the road traffic emissions have relatively minor influence on the SOA mass concentrations in Europe (figure 10), and even a minor net negative contribution to the SOA mass in regions with intense road traffic. The main reason for this is that the road traffic has high NO_x and relatively low and slowly oxidising VOC emissions which results in delayed SOA formation. The NO_x emissions results in complex non-linear effects on the atmospheric chemistry that governs not only the oxidation of the emitted anthropogenic VOCs, but also the oxidation of biogenic VOCs. According to the model simulations this leads to supressed biogenic secondary organic aerosols (BSOA) and anthropogenic secondary organic aerosols (ASOA) formation in regions in central and southern Europe where the most intense road traffic emissions occur (figure 10C-D).

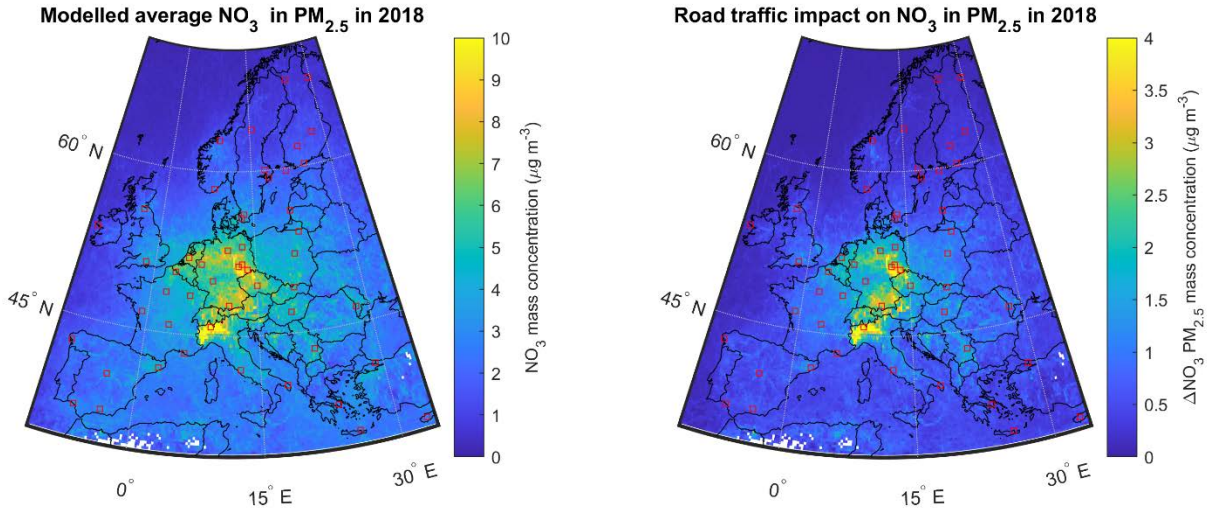

***Figure 8**. Modelled average nitrate mass contribution to the $PM_{2.5}$ levels in Europe in the year 2018. Panel **A** shows the absolute concentrations from the Basecase model simulations. Panel **B** shows the concentration difference between the Basecase and the WoRoad simulations.*

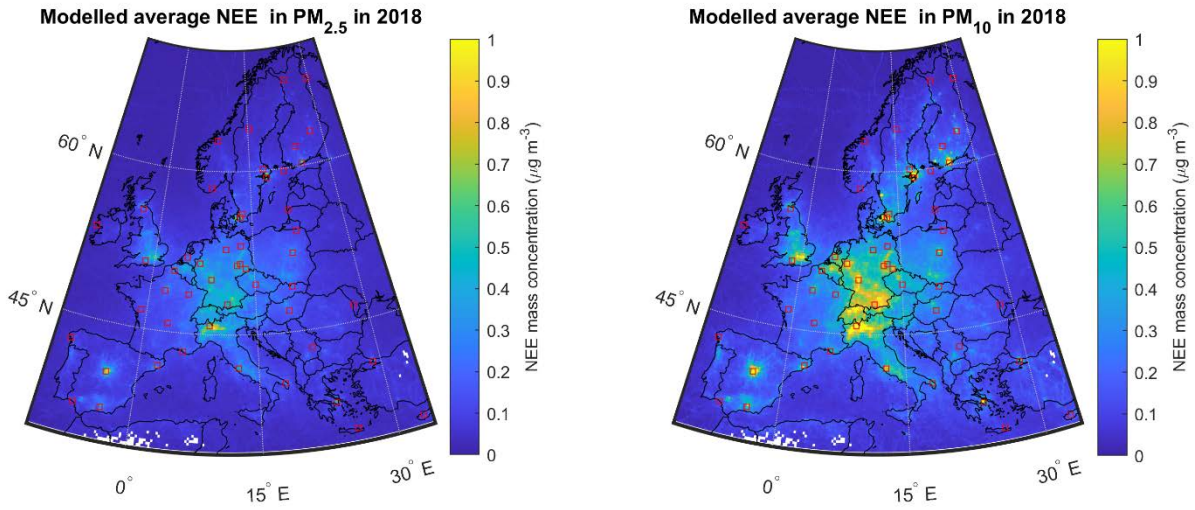

Figure 9. *Modelled average NEE particle mass contribution using the HTPAv3 road traffic non-exhaust emission inventory. Panel **A** shows the NEE in $PM_{2.5}$ and panel **B** the NEE in PM_{10} in Europe in the year 2018.*

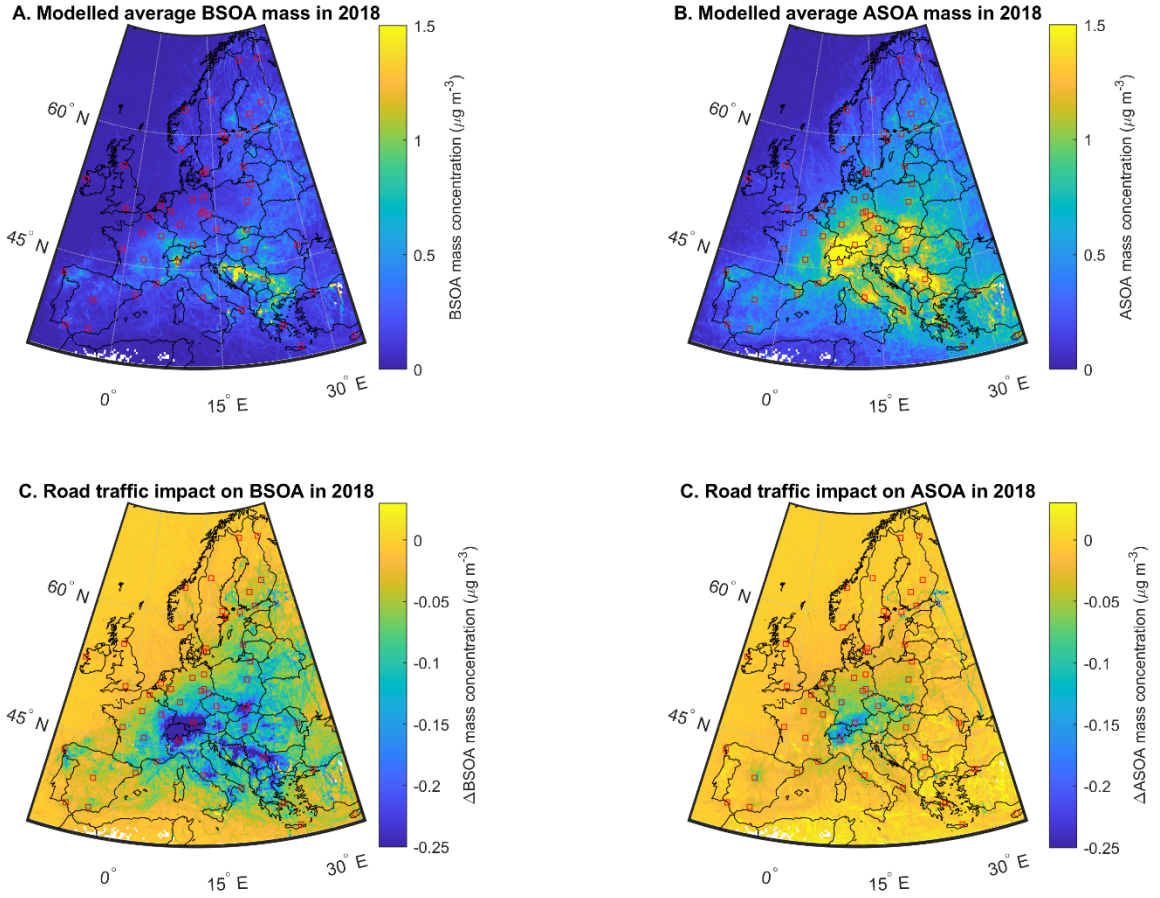

Figure 10. *Modelled yearly average BSOA (panel **A**) and ASOA (panel **B**) over Europe in 2018. Panels **C** and **D** show the difference in the modelled BSOA and ASOA concentrations between the Basecase and WoRoad simulations. Negative values indicate that road transport emissions have a net negative impact on the yearly average SOA mass concentrations.*

5. Outlook

The modelled yearly average $PM_{2.5}$ levels in Europe have been prepared to be used to assess the population exposure and health impacts, with focus on mortality and certain symptoms and diseases. The Health Impact Assessment (HIA) will be done primarily for transport sectors' exhaust emissions, and for primary and secondary PM separately. Additionally, the HIA will be separated based on organic and inorganic PM. The modelled $PM_{2.5}$ levels will be combined with the JRC-GEOSTAT 2018, reporting the number of residents for the year 2018 for Europe. The vehicle emissions impact on the population health will also be transformed to economical costs.

Several urban regions in Europe, e.g. Leipzig, Dresden and Helsinki have continuous observations of PNSD at both urban background and urban street stations. Thus, for these cities it is possible to evaluate the modelled PNSD both at urban background and at street level. We know that the modelled relatively coarse resolution European scale concentration fields that are presented in this report generally underestimate the particle concentrations in urban regions, especially at polluted traffic sites. To address this model bias, we plan to run ADCHEM specifically for the Helsinki region for one complete calendar year using a high-resolution anthropogenic emission inventory for the Nordic countries (Paunu et al., 2024). From the simulations we will derive high-resolution (~1 km^2) maps of UFP, SOA, POA, BC etc. over the urban regions and compare them with the coarser resolution European scale model simulations. We will specifically investigate how the size resolved aerosol chemical and physical properties are influenced by the local and regional road traffic, harbors and airports.

The aerosol particle-induced generation of reactive oxygen species (ROS) is linked to health risks, such as respiratory diseases, DNA damage, mutations and cancer. Particles also cause inflammation, which is an indirect route to ROS formation and oxidative stress. PM oxidative potential (OP) is the capacity of PM to oxidize molecules in biological tissues or cells directly by oxidants that are present on and/or within PM (PM bound ROS) and indirectly by the catalytic generation of ROS in vivo via cellular redox reactions (Zhang et al., 2022). The sources and levels of PM oxidative potential in Europe have previously been assessed using offline OP acellular assays. The results highlight the importance of non-exhaust road-transport emissions (NEE), ASOA, BSOA, biomass burning OA (BBOA) and POA from vehicles (HOA) as sources of OP that the population are exposed to (Daellenbach et al., 2020). Epidemiological and HIA studies presently link particle concentrations, via population exposure, directly to health effects, without considering inhaled dose, and this contributes to substantial uncertainty in their ability to compare health effects from different types of emissions. The dose estimates may also reduce noise in epidemiological studies as it is ultimately the inhaled deposited dose that causes the effects. Based on the detailed size resolved particle chemical and physical properties from ADCHEM we plan to estimate the respiratory tract deposited doses of hundreds of different compounds and the dose of both PM bound ROS and ROS induced in vivo OP in different regions of the respiratory system among the population in Europe.

6. References

Amann, M., Bertok, I., Borken-Kleefeld, J., Cofala, J., Heyes, C., Höglund-Isaksson, L., Klimont, Z., Nguyen, B., Posch, M., Rafaj, P., Sandler, R., Schöpp, W., Wagner, F., Winiwarter, W.: Cost-effective control of air quality and greenhouse gases in Europe: Modelling and policy applications, *Environmental Modelling and Software*, 26, 1489-1501, 2011.

Bergman, T., Makkonen, R., Schrödner, R., Swietlicki, E., Phillips, V. T. J., Le Sager, P., and van Noije, T.: Description and evaluation of a secondary organic aerosol and new particle formation scheme within TM5-MP v1.2, *Geosci. Model Dev*., 15, 683–713, https://doi.org/10.5194/gmd-15-683-2022, 2022.

Bloss, C., Wagner, V., Jenkin, M. E., Volkamer, R., Bloss, W. J., Lee, J. D., Heard, D. E., Wirtz, K., Martin-Reviejo, M., Rea, G., Wenger, J. C., and Pilling, M. J.: Development of a detailed chemical mechanism (MCMv3.1) for the atmospheric oxidation of aromatic hydrocarbons, *Atmos. Chem. Phys*., 5, 641–664, https://doi.org/10.5194/acp-5-641-2005, 2005.

Crippa, M., Guizzardi, D., Butler, T., Keating, T., Wu, R., Kaminski, J., Kuenen, J., Kurokawa, J., Chatani, S., Morikawa, T., Pouliot, G., Racine, J., Moran, M. D., Klimont, Z., Manseau, P. M., Mashayekhi, R., Henderson, B. H., Smith, S. J., Suchyta, H., Muntean, M., Solazzo, E., Banja, M., Schaaf, E., Pagani, F., Woo, J.-H., Kim, J., Monforti-Ferrario, F., Pisoni, E., Zhang, J., Niemi, D., Sassi, M., Ansari, T., and Foley, K.: The HTAP_v3 emission mosaic: merging regional and global monthly emissions (2000–2018) to support air quality modelling and policies, *Earth Syst. Sci. Data*, 15, 2667–2694, https://doi.org/10.5194/essd-15-2667-2023, 2023.

Daellenbach, K. R., Uzu, G., Jiang, J., Cassagnes, L.-E., Leni, Z., Vlachou, A., Stefenelli, G., Canonaco, F., Weber, S., Segers, A., Kuenen, J. J. P., Schaap, M., Favez, O., Albinet, A., Aksoyoglu, S., Dommen, J., Baltensperger, U., Geiser, M., El Haddad, I., Jaffrezo, J.-L., and Prévôt, A. S. H.: Sources of particulate-matter air pollution and its oxidative potential in Europe, *Nature*, 587, 414–419, https://doi.org/10.1038/s41586-020-2902-8, 2020

Eriksson, A. C., Wittbom, C., Roldin, P., Sporre, M., Öström, E., Nilsson, P., Martinsson, J., Rissler, J., Nordin, E. Z., Svenningsson, B., Pagels J., and Swietlicki, E.: Diesel soot aging in urban plumes within hours under cold dark and humid conditions, *Sci Rep* 7, Article number: 12364, 2017.

Granier, C., Darras, S., Denier van der Gon, H. Doubalova, J., Elguindi, N., Galle, B., Gauss, M., Guevara, M., Jalkanen, J.-P., Kuenen, J., Liousse, C., Quack, B., Simpson, D., Sindelarova, K.: The Copernicus Atmosphere Monitoring Service global and regional emissions (April 2019 version), *Copernicus Atmosphere Monitoring Service (CAMS) report*, doi:10.24380/d0bn-kx16, 2019.

Hoppel, W. A.; Frick, G. M.; Larson, R. E.: Effect of Nonprecipitating Clouds on the Aerosol Size Distribution in the Marine Boundary Layer. *Geophys. Res. Lett*. 1986, 13, 125−128.

Iyer, S., Kumar, A., Savolainen, A., Barua, S, Daub, C., Pichelstorfer, L., Roldin, P., Garmash, O., Seal, P., Kurtén, T. and Rissanen, M.: Molecular rearrangement of bicyclic peroxy radicals is a key route to aerosol from aromatics. *Nat Commun* 14, 4984, 2023

Jenkin, M. E., Saunders, S. M., and Pilling, M. J.: The tropospheric degradation of volatile organic compounds: a protocol for mechanism development, *Atmos. Environ*., 31, 81–104, 1997.

Jenkin, M. E., Saunders, S. M., Wagner, V., and Pilling, M. J.: Protocol for the development of the Master Chemical Mechanism, MCMv3(Part B): tropospheric degradation of aromatic volatile organic compounds, *Atmos. Chem. Phys*., 3, 181–193, 2003

Jenkin, M. E., Wyche, K. P., Evans, C. J., Carr, T., Monks, P. S., Alfarra, M. R., Barley, M. H., McFiggans, G. B., Young, J. C., and Rickard, A. R.: Development and chamber evaluation of the MCM v3.2 degradation scheme for β-caryophyllene, *Atmos. Chem. Phys*., 12, 5275–5308, https://doi.org/10.5194/acp-12-5275-2012, 2012.

Jenkin, M. E., Young, J. C., and Rickard, A. R.: The MCM v3.3.1 degradation scheme for isoprene, *Atmos. Chem. Phys*., 15, 11433–11459, https://doi.org/10.5194/acp-15-11433-2015, 2015.

Linell, J., Isaxon, C., Olsson, B., Stroh, E., Wollmer, P., Löndahl, J., and Rissler, J.: Effects of breathing variables on modelled particle lung deposition at physical activity for children and adults. *Air Qual Atmos Health* **17**, 843–856, https://doi.org/10.1007/s11869-023-01484-0, 2024.

Lintusaari, H., Kuuluvainen, H., Vanhanen, J., Salo, L., Portin, H., Järvinen, A., Juuti, P., Hietikko, R., Teinilä, K., Timonen, H., Niemi, J. V., and Rönkkö, T.: Sub-23 nm Particles Dominate Non-Volatile Particle Number Emissions of Road Traffic, *Environmental Science & Technology*, 57 (29), 10763-10772 DOI: 10.1021/acs.est.3c03221, 2023.

Luo, Y., Thomsen, D., Iversen, E. M., Roldin, P., Skønager, J. T., Li, L., Priestley, M., Pedersen, H. B., Hallquist, M., Bilde, M., Glasius, M., and Ehn, M.: Formation and temperature dependence of highly oxygenated organic molecules (HOMs) from Δ3-carene ozonolysis, *Atmos. Chem. Phys*., 24, 9459–9473, https://doi.org/10.5194/acp-24-9459-2024, 2024.

Nie,W., Yan, C., Yang, L., Roldin, P., Liu, Y., Vogel, A. L., Molteni,U., Stolzenburg, D., Finkenzeller, H., Amorim, A., Bianchi, F.,Curtius, J., Dada, L., Draper, D. C., Duplissy, J., Hansel, A., He,X.-C., Hofbauer, V., Jokinen, T., Kim, C., Lehtipalo, K., Nichman,L., Mauldin, R. L., Makhmutov, V., Mentler, B., Mizelli-Ojdanic, A., Petƒjƒ, T., Qu..l...ver, L. L. J., Schallhart, S., Simon,M., Tauber, C., Tom..„ A., Volkamer, R., Wagner, A. C., Wagner,R., Wang, M., Ye, P., Li, H., Huang, W., Qi, X., Lou, S., Liu, T.,Chi, X., Dommen, J., Baltensperger, U., El Haddad, I., Kirkby,J., Worsnop, D., Kulmala, M., Donahue, N. M., Ehn, M., andDing, A.: NO at low concentration can enhance the formation of highly oxygenated biogenic molecules in the atmosphere, *Nat. Commun*., 14, 3347, https://doi.org/10.1038/s41467-023-39066-4, 2023.

Ng, N. L., Kroll, J. H., Chan, A. W. H., Chhabra, P. S., Flagan, R. C., and Seinfeld, J. H.: Secondary organic aerosol formation from *m*-xylene, toluene, and benzene, *Atmos. Chem. Phys*., 7, 3909–3922, https://doi.org/10.5194/acp-7-3909-2007, 2007.

Olenius, T., Kupiainen-Maatta, O., Ortega, I. K., Kurten, T., and Vehkamaki, H.: Free energy barrier in the growth of sulfuric acid‐ammonia and sulfuric acid‐dimethylamine clusters, *The Journal of Chemical Physics*, 139, 084 312, https://doi.org/10.1063/1.4819024, 2013

Olenius, T. and Roldin P.: Role of gas–molecular cluster–aerosol dynamics in atmospheric new particle formation, *Sci Rep*, 12:10135, 2022.

Olin, M., Oikarinen, H., Marjanen, P., Mikkonen, S., and Karjalainen, P.: High Particle Number Emissions Determined with Robust Regression Plume Analysis (RRPA) from Hundreds of Vehicle Chases, *Environmental Science & Technology*, 57 (24), 8911-8920, DOI: 10.1021/acs.est.2c08198, 2023.

Paunu, V.-V., Karvosenoja, N., Segersson, D., López-Aparicio, S., Nielsen, O.-K., Schmidt Plejdrup, M., Thorsteinsson, T., Vo, D. T., Kuenen, J., Denier van der Gon, H., Jalkanen, J.-P., Brandt, J., and Geels, C.: Air pollution emission inventory using national high-resolution spatial parameters for the Nordic countries and analysis of $PM_{2.5}$ spatial distribution for road transport and machinery and off-road sectors, *Earth Syst. Sci. Data*, 16, 1453–1474, https://doi.org/10.5194/essd-16-1453-2024, 2024.

Pichelstorfer, L., Roldin, P., Rissanen, M., Hyttinen, N., Garmash, O, Xavier, C., Zhou, P., Clusius, P. Foreback, B., Almeida, T. G., Deng, C. J., Baykara, M. Kurtén, T. Boy, M.: Towards automated inclusion of autoxidation chemistry in models: from precursors to atmospheric implications, *Environ. Sci.: Atmos*., 4 (8), 879-896, http://dx.doi.org/10.1039/D4EA00054D, 2024.

Roldin, P., Swietlicki, E., Schurgers, G., Arneth, A., Lehtinen, K. E. J., Boy, M., and Kulmala, M.: Development and evaluation of the aerosol dynamics and gas phase chemistry model ADCHEM, *Atmos. Chem. Phys.*, 11, 5867-5896, 2011a.

Roldin, P., Swietlicki, E., Massling, A., Kristensson, A., Löndahl, J., Eriksson, A., Pagels, J., and Gustafsson, S.: Aerosol ageing in an urban plume – implication for climate, *Atmos. Chem. Phys.*, 11, 5897–5915, 2011b.

Roldin, P., Ehn, M., Kurtén, T., Olenius, T., Rissanen, M. P., Sarnela, N., Elm, J., Rantala, P., Hao, L., Hyttinen, N., Heikkinen, L., Worsnop, D. R., Pichelstorfer, L., Xavier, C., Clusius, P., Öström, E., Petäjä, T., Kulmala, M., Vehkamäki, H., Virtanen, A., Riipinen, I., and Boy, M.: The role of highly oxygenated organic molecules in the Boreal aerosol-cloudclimate system, *Nat Commun*, 10, 4370, 2019.

Saunders, S. M., Jenkin, M. E., Derwent, R. G., and Pilling, M. J.: Protocol for the development of the Master Chemical Mechanism, MCM v3 (Part A): tropospheric degradation of non-aromatic volatile organic compounds, *Atmos. Chem. Phys*., 3, 161–180, https://doi.org/10.5194/acp-3-161-2003, 2003.

Stein, A. F. Draxler, R. R. Rolph, G. D., Stunder, B. J. B., Cohen M. D. and Ngan, F.: NOAA's HYSPLIT Atmospheric Transport and Dispersion Modeling System. *BAMS*, DOI: https://doi.org/10.1175/BAMS-D-14-00110.1, 2059–2077, 2015.

Srivastava, D., Vu, T.V., Tong, S., Shi, Z., and Harrision, R. M. Formation of secondary organic aerosols from anthropogenic precursors in laboratory studies. *npj Clim Atmos Sci* 5, 22, https://doi.org/10.1038/s41612-022-00238-6, 2022.

Svenhag, C., Sporre, M. K., Olenius, T., Yazgi, D., Blichner, S. M., Nieradzik, L. P., and Roldin, P.: Implementing detailed nucleation predictions in the Earth system model EC-

Earth3.3.4: sulfuric acid–ammonia nucleation, *Geosci. Model Dev*., 17, 4923–4942, https://doi.org/10.5194/gmd-17-4923-2024, 2024a.

Svenhag, C., Roldin, P., Olenius, T., Wollesen de Jonge, R., Blichner, S., Yazgi, D., and Sporre, M.: Seasonal differences in observed versus modeled new particle formation over boreal regions, *EGUsphere* [preprint], https://doi.org/10.5194/egusphere-2024-3626, 2024b.

van Noije, T. P., Le Sager, P., Segers, A. J., van Velthoven, P. F., Krol, M. C., Hazeleger, W., Williams, A. G., and Chambers, S. D.: Simulation of tropospheric chemistry and aerosols with the climate model EC-Earth, *Geoscientific Model Development*, 7, 2435–2475, https://doi.org/10.5194/gmd-7-2435-2014, 2014.

Vartiainen, A., Roldin, P., Irfan, M., Thomasson, A., Kokkola, H., and Yli-Juuti, T.: Correcting the bias between simple and complex monoterpene oxidation schemes with neural networks – Defining the variable space, Report Series in Aerosol Science *No. 280, Abstract Book of the ACCC-FASN Science Conference*, pp 255-256, ISBN 978-952-7507-37-7, 2024.

Vignati, E., Wilson, J., and Stier, P.: M7: An efficient size-resolved aerosol microphysics module for large-scale aerosol transport models, *Journal of Geophysical Research: Atmospheres*, 109, https://doi.org/10.1029/2003jd004485, 2004

Wollesen de Jonge, R., Xavier, C., Olenius, T., Elm, J., Svenhag, C., Hyttinen, N., Nieradzik, L., Sarnela, N., Kristensson, A., Petäjä, T., Ehn, M. and Roldin, P.: *Environmental Science & Technology 58* (25), 10956-10968 DOI: 10.1021/acs.est.4c01891, 2024.

Xavier, C., Wollesen de Jonge, R., Jokinen, T., Beck, L., Sipilä, M., Olenius, T. and Roldin, P.: Role of iodine-assisted aerosol particle formation in Antarctica, *Environmental Science & Technology* 58 (17), 7314-7324, DOI: 10.1021/acs.est.3c09103, 2024.

Zhang, Z.-H., Hartner, E., Utinger, B., Gfeller, B., Paul, A., Sklorz, M., Czech, H., Yang, B. X., Su, X. Y., Jakobi, G., Orasche, J., Schnelle-Kreis, J., Jeong, S., Gröger, T., Pardo, M., Hohaus, T., Adam, T., Kiendler-Scharr, A., Rudich, Y., Zimmermann, R., and Kalberer, M.: Are reactive oxygen species (ROS) a suitable metric to predict toxicity of carbonaceous aerosol particles?, *Atmos. Chem. Phys*., 22, 1793–1809, https://doi.org/10.5194/acp-22-1793-2022, 2022.